
Efficient GNN Explanation via Learning Removal-based Attribution

Yao Rong¹, Guanchu Wang², Qizhang Feng³, Ninghao Liu⁴, Zirui Liu²,
Enkelejda Kasneci¹, Xia Hu²

¹Technical University of Munich, ²Rice University

³Texas A&M University, ⁴University of Georgia

{yao.rong, enkelejda.kasneci}@tum.de, {guanchu.wang, z1105, xia.hu}@rice.edu

qf31@tamu.edu, ninghao.liu@uga.edu

Abstract

As Graph Neural Networks (GNNs) have been widely used in real-world applications, model explanations are required not only by users but also by legal regulations. However, simultaneously achieving high fidelity and low computational costs in generating explanations has been a challenge for current methods. In this work, we propose a framework of GNN explanation named LeArn Removal-based Attribution (LARA) to address this problem. Specifically, we introduce removal-based attribution and demonstrate its substantiated link to interpretability fidelity theoretically and experimentally. The explainer in LARA learns to generate removal-based attribution which enables providing explanations with high fidelity. A strategy of subgraph sampling is designed in LARA to improve the scalability of the training process. In the deployment, LARA can efficiently generate the explanation through a feed-forward pass. We benchmark our approach with other state-of-the-art GNN explanation methods on six datasets. Results highlight the effectiveness of our framework regarding both efficiency and fidelity. In particular, LARA is $3.5\times$ faster and achieves higher fidelity than the state-of-the-art method on the large dataset ogbn-arxiv (more than 160K nodes and 1M edges), showing its great potential in real-world applications. Our source code is available at <https://anonymous.4open.science/r/LARA-10D8/README.md>.

1 Introduction

Graph Neural Networks (GNNs) achieve great success in many areas, while their black-box nature limits their applications where a trustworthy decision is needed, such as in recommender systems [32], social networks [10], and biochemical or medical analysis [33]. In many scenarios, it is therefore important to explain the behavior of GNNs due to the requirement of both stakeholders and regulations. For instance, according to the European Union General Data Protection Regulation [13], commercial recommender systems should provide users with explanations along with recommendations.

In recent years, various methods have been proposed for GNN explanation [38]. There are two major aspects for evaluating the real-world applicability of an explanation method: **fidelity** [38, 20, 40, 27] and **efficiency** [5, 31, 4, 22, 21]. The fidelity reflects the faithfulness of explanation [38], and the efficiency indicates the latency of a method deployed to real-world scenarios [5]. To generate faithful explanations, existing approaches rely on a searching process of input subgraph that can minimize the variance of GNN output [20, 11]. However, these pieces of work suffer from the time-consuming process of searching the explanations. For instance, to obtain an explanation, GNNExplainer [36] requires learning a mask of input neighbors; ZORRO [12] and SubgraphX [37] utilize on greedy algorithms and Monte Carlo Tree Search to sample important subgraph that can maximize the

designed objective function. Either the learning or searching overhead can significantly slow down the process of explanation generation, which limits their application to real-time scenarios. This is particularly relevant in social network graphs that frequently consist of millions of nodes and edges.

In order to provide efficient GNN explanations, previous work [24, 18, 30, 4] attempts to train a deep neural network-based explainer, amortizing the time and resource cost of generating explanations of many samples. However, it is quite challenging to ensure the faithfulness/fidelity of explanations due to the absence of “ground-truth explanations” to provide the supervision of faithfulness in the training process. Existing work suggests maximizing the mutual information (MI) between the prediction made using learnable explanatory subgraphs and the original graphs, but the MI value fails to be consistent with the interpretation fidelity, especially on large graph datasets where the number of neighbors increases. Another challenge is to design a scalable training process considering the limited memory capacity of computational units (GPU), as training the explainer requires huge memory to store the graph structure for aggregation operation. Training on large graphs should be deployed with optimization to avoid exceeding the memory capacity.

To bridge this research gap, we propose a framework **LeArN Removal-based Attribution (LARA)** towards efficient and faithful GNN explanation. Specifically, we first experimentally demonstrate the MI value becomes less correlated with fidelity as the number of neighbors grows. Thus, we propose removal-based attribution for GNN explanation, and demonstrate its contribution to the high fidelity of interpretation from both theoretical and empirical perspectives. Then, we develop an amortized explainer to learn the removal-based attribution, such that it can efficiently generate GNN explanation in a feed-forward process on complex graph structures. Finally, we design a strategy of subgraph sampling in cooperation with the training of explainer to improve its scalability on large graphs. Experiments on six benchmark datasets demonstrate the effectiveness of LARA regarding fidelity, efficiency, and scalability.

The ever-growing real-world social graphs can have more than millions of nodes and edges, poses significant challenges for the efficiency and scalability of GNN explanation approaches. According to the overall evaluation of fidelity and efficiency in Figure 1, on the ogbn-arxiv dataset with over 160K nodes and 1M edges, **LARA achieves a $3.5\times$ speedup as well as higher interpretation fidelity** than the state-of-the-art approach. This indicates the significant potential of our work for real-world applications. To summarize, our work makes the following contributions:

- We experimentally study the inconsistency of mutual information with interpretation fidelity as the number of neighbors increases. We propose removal-based attribution for GNN explanation, and demonstrate its contribution to high fidelity from both theoretical and experimental perspectives.
- We propose a framework LARA which deploys an amortized explainer for efficient GNN explanation generation. The learning of the explainer incorporates the proposed removal-based attribution towards fidelity maximization, along with a subgraph sampling strategy for training scalability.
- We benchmark LARA on six datasets including a real-world large graph dataset, in comparison with state-of-the-art methods. The experiment results demonstrate the effectiveness of LARA in terms of fidelity, efficiency, and scalability.

2 Preliminaries

In this section, we introduce the notations for the problem formulation and evaluation metrics that motivate the design of our GNN explanation framework.

2.1 Notations

We consider an arbitrary black-box GNN $f(\cdot)$ as the target model to be explained. The GNN model $f(\cdot)$ is trained on the graph $\mathcal{G} = (\mathcal{V}, \mathcal{E})$, where $\mathcal{V} = \{v_1, \dots, v_N\}$ and \mathcal{E} denote the node set and

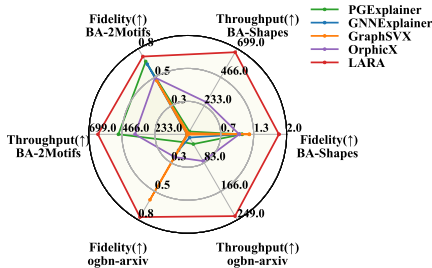


Figure 1: Comparison of LARA with state-of-the-art GNN explanations in fidelity and efficiency on the BA-2Motifs (graph classification), BA-Shapes (node classification), and ogbn-arxiv (node classification). Experimental details in this figure are given in Appendix C.

edge set, respectively; $N = |\mathcal{V}|$ is the number of nodes in the graph. For any node subset $\mathcal{S} \subseteq \mathcal{V}$, let $\mathcal{G}_{\mathcal{S}} = \{\mathcal{S}, \mathcal{E}_{\mathcal{S}}\}$ denote the subgraph which consists of the nodes in \mathcal{S} and the related edges $\mathcal{E}_{\mathcal{S}}$, where $\mathcal{E}_{\mathcal{S}}$ represents the edges connecting the nodes in \mathcal{S} . For each node $v_i \in \mathcal{V}$, let $\mathcal{N}(v_i)$ denote the neighbors of node v_i including itself (as the zero-hop neighbor). Thus, $\mathcal{G}_{\mathcal{N}(v_i)} = \{\mathcal{N}(v_i), \mathcal{E}_{\mathcal{N}(v_i)}\}$ denotes the subgraph containing the neighbors of v_i and their associated edges; and $f(\mathcal{G}_{\mathcal{N}(v_i)})$ aggregates the information from its neighbors to make the prediction of node v_i . In this work, we focus on estimating the attribution of each neighbor $v_j \in \mathcal{N}(v_i)$ to the GNN prediction $f(\mathcal{G}_{\mathcal{N}(v_i)})$.

2.2 Explanation Evaluation Metrics

Fidelity. We follow existing work [38, 40, 20] to consider Fidelity^+ and Fidelity^- as the metrics to evaluate GNN explanation in this work. Concretely, fidelity reflects the faithfulness of explanations [29, 35, 1], which can be widely applied to scenarios where ground truth explanations are not available. Formally, given the important neighbors $\mathcal{N}_{v_i}^* \subseteq \mathcal{N}(v_i)$ of a node v_i discovered by an explanation method, $\mathcal{G}_{\mathcal{N}_{v_i}^*}$ denotes the subgraph consisting of the important nodes $\mathcal{N}_{v_i}^*$ and the associated edges. Likewise, $\mathcal{G}_{\mathcal{N}(v_i) \setminus \mathcal{N}_{v_i}^*}$ represents the subgraph after removing the important nodes $\mathcal{N}_{v_i}^*$ and their associated edges from $\mathcal{G}_{\mathcal{N}(v_i)}$, i.e., unimportant nodes are preserved in $\mathcal{N}(v_i) \setminus \mathcal{N}_{v_i}^*$.

Fidelity^+ evaluates the explanation method via *removing the important neighbors* and checking the model prediction changes. Therefore, Fidelity^+ is defined as:

$$\uparrow \text{Fidelity}^+ = \frac{1}{N} \sum_{i=1}^N f(\mathcal{G}_{\mathcal{N}(v_i)}) - f(\mathcal{G}_{\mathcal{N}(v_i) \setminus \mathcal{N}_{v_i}^*}), \quad (1)$$

where $f(\mathcal{G}_{\mathcal{N}(v_i)}) - f(\mathcal{G}_{\mathcal{N}(v_i) \setminus \mathcal{N}_{v_i}^*}) \triangleq \text{Fidelity}^+(v_i, \mathcal{N}_{v_i}^*)$ represents the Fidelity^+ of the explanatory nodes $\mathcal{N}_{v_i}^*$ for a single node v_i ; and N refers to the number of nodes in the graph. Higher Fidelity^+ indicates a better explanation, because the discriminative neighbors of each node are recognized and removed, resulting in huge prediction changes.

On the other hand, Fidelity^- evaluates the GNN explanation via *removing the trivial neighbors* of each node. Thus, Fidelity^- is formalized as follows:

$$\downarrow \text{Fidelity}^- = \frac{1}{N} \sum_{i=1}^N f(\mathcal{G}_{\mathcal{N}(v_i)}) - f(\mathcal{G}_{\mathcal{N}_{v_i}^*}), \quad (2)$$

where $f(\mathcal{G}_{\mathcal{N}(v_i)}) - f(\mathcal{G}_{\mathcal{N}_{v_i}^*}) \triangleq \text{Fidelity}^-(v_i, \mathcal{N}_{v_i}^*)$ refers to the Fidelity^- for a single node v_i . Lower Fidelity^- implies a better explanation, since the contributive neighbors of each node have been preserved to keep the prediction similar to the original one.

Throughput. Following existing work [4, 31, 22], we utilize algorithmic throughput to evaluate the efficiency of explanation methods. Specifically, the throughput is defined as $N_{\text{test}}/t_{\text{test}}$, where N_{test} is the number of instances being explained, and t_{test} represents the total time cost of the explanation process. Thus, the throughput indicates the number of instances being explained per second, and a higher throughput implies a more efficient explanation method.

3 Removal-based Attribution

In this section, we first demonstrate the limitation of using mutual information (MI) as guidance for faithful GNN explanation generation in existing methods. Then, we define removal-based attribution and theoretically demonstrate its consistency with the expected interpretation fidelity. Finally, we experimentally show the correlation between fidelity and removal-based attribution.

Many existing work trains an explainer by a loss adopted from MI (e.g., MI with regularization [24] or the causal counterpart of MI [19]), so that the trained explainer provides explanatory features (e.g., edge importance) based on the MI value in the objective function. However, we found the MI value becomes less consistent with the interpretation fidelity as the number of neighbor nodes increases. To illustrate this issue, we conduct a preliminary experiment on the dataset BA-Community [36] and ogbn-arxiv [14], and visualize the correlation of the interpretation fidelity with the MI value for the

target nodes with different numbers of neighbors in Figure 2. The details about the experiment are given in Appendix A. It is observed in Figure 2 (a) that the MI value is approximately correlated with fidelity as the number of neighbors is small. However, as the number of neighbors grows on the dataset obgn-arxiv, this correlation becomes less evident in Figure 2 (b), indicating the unfaithfulness of using MI value as explanations on larger graphs.

To address the limitation of MI value, we propose removal-based attribution that consistently reflects fidelity. Specifically, we combine two fidelity metrics Fidelity^+ and Fidelity^- given by Equations (1) and (2) into a hybrid formulation of fidelity as follows:

$$\Delta\text{Fidelity}(v_i, \mathcal{N}_{v_i}^*) = \text{Fidelity}^+(v_i, \mathcal{N}_{v_i}^*) - \text{Fidelity}^-(v_i, \mathcal{N}_{v_i}^*). \quad (3)$$

Note that the estimation in Equation (3) is considered for a neighbor node set $\mathcal{N}_{v_i}^*$. We extend Equation (3) to the case of each single neighbor node $v_j \in \mathcal{N}(v_i)$ by considering the expected fidelity $\mathbb{E}_{\mathcal{S}_j \subseteq \mathcal{N}(v_i)}[\Delta\text{Fidelity}(v_i, \mathcal{S}_j)]$, where the enumeration of $\mathcal{S}_j \subseteq \mathcal{N}(v_i)$ satisfies $\mathcal{S}_j \ni v_j$. Without loss of generality, we give Theorem 3.1 to demonstrate the consistency of expected fidelity with the expected GNN prediction difference. The proof of Theorem 3.1 is given in Appendix B.

Theorem 3.1. *For a target node v_i and one of its neighbors v_j , let $\phi_{j \rightarrow i} = \mathbb{E}_{\mathcal{S}_j \subseteq \mathcal{N}(v_i)}[f(\mathcal{G}_{\mathcal{S}_j}) - f(\mathcal{G}_{\mathcal{N}(v_i) \setminus \mathcal{S}_j})]$. Generally, $\forall \mathcal{J} \subseteq \mathcal{N}(v_i)$, if $\exists \mathcal{J}^* \subseteq \mathcal{N}(v_i)$ satisfying $\mathbb{E}_{j \sim \mathcal{J}} \phi_{j \rightarrow i} \leq \mathbb{E}_{j \sim \mathcal{J}^*} \phi_{j \rightarrow i}$, then*

$$\mathbb{E}_{j \sim \mathcal{J}} \mathbb{E}_{\mathcal{S}_j \subseteq \mathcal{N}(v_i)}[\Delta\text{Fidelity}(v_i, \mathcal{S}_j)] \leq \mathbb{E}_{j \sim \mathcal{J}^*} \mathbb{E}_{\mathcal{S}_j \subseteq \mathcal{N}(v_i)}[\Delta\text{Fidelity}(v_i, \mathcal{S}_j)]. \quad (4)$$

According to Theorem 3.1, if the expected prediction difference of a node subset \mathcal{J}^* is larger than that of any node subset \mathcal{J} , then the expected fidelity of the node subset \mathcal{J}^* is also larger than that of any node subset. As we aim at a node subset that maximizes the fidelity, the objective can be altered to find such a node subset \mathcal{J}^* for the target node v_i through $\mathbb{E}_{j \sim \mathcal{J}} \phi_{j \rightarrow i}$.

Formally, we define $\phi_{j \rightarrow i}$ as the *removal-based attribution* for each neighbor v_j of the target node v_i to indicate its importance to the GNN prediction $f(\mathcal{G}_{\mathcal{N}(v_i)})$ in Definition 3.2.

Definition 3.2 (Removal-based Attribution). For a target node v_i and neighbor node v_j , the removal-based attribution $\phi_{j \rightarrow i}$ is defined as

$$\phi_{j \rightarrow i} = \mathbb{E}_{\mathcal{S}_j \subseteq \mathcal{N}(v_i)}[f(\mathcal{G}_{\mathcal{S}_j}) - f(\mathcal{G}_{\mathcal{N}(v_i) \setminus \mathcal{S}_j})] = \frac{1}{2^{|\mathcal{N}(v_i)|-1}} \sum_{\mathcal{S}_j \subseteq \mathcal{N}(v_i)} f(\mathcal{G}_{\mathcal{S}_j}) - f(\mathcal{G}_{\mathcal{N}(v_i) \setminus \mathcal{S}_j}). \quad (5)$$

According to the numerical result in Figure 2 (c). A stronger correlation can be observed between the interpretation fidelity with our proposed removal-based attribution. This indicates the advantage of utilizing removal-based attribution as node attribution in GNN explanations.

4 Learn Removal-based Attribution (LARA)

We introduce details of the proposed LARA framework in this section. As illustrated in Figure 3, LARA learns a GNN-based explainer on a training dataset, where the details of explainer training and training sample collection are given in Section 4.1, and Section 4.2, respectively.

4.1 Explainer Training

We introduce how the amortized explainer in LARA generates the removal-based attribution in this section. Different from existing work of amortized explainers on the regular data [17, 6, 4], graphs

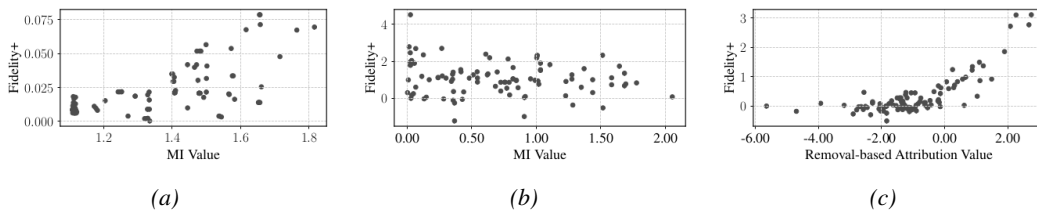


Figure 2: (a) Correlation between fidelity and mutual information value on the BA-Community and (b) obgn-arxiv datasets; (c) Correlation between fidelity and removal-based attribution on the obgn-arxiv dataset.

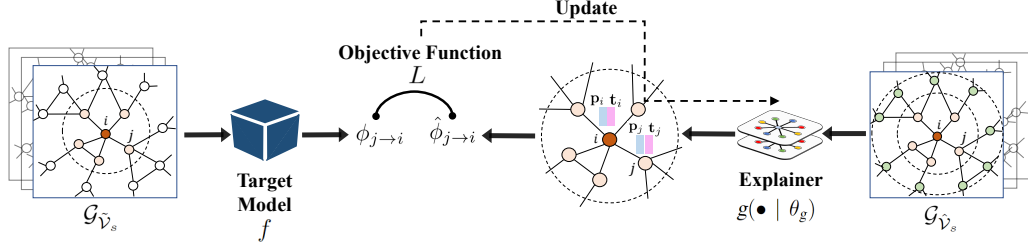


Figure 3: The framework of LARA. **Left:** Subgraphs are sampled to estimate the removal-based attribution $\phi_{j \rightarrow i}$. **Right:** $g(\bullet | \theta_g)$ samples subgraphs as input and generates the node attribution $\hat{\phi}_{j \rightarrow i}$ based on the source embedding \mathbf{p}_j and target embedding \mathbf{t}_i . **Middle:** The parameters of the amortized explainer are updated via optimizing the training objective given by Equation (8).

are irregular and non-Euclidean data, where the number of nodes and edges vary in different graph regions, and each node may have a different number of neighbors. LARA adopts a GNN-based amortized explainer $g(\bullet | \theta_g)$ to solve this problem. Specifically, for a node $v_i \in \mathcal{G}$, $g(\bullet | \theta_g)$ generates explanation-oriented embeddings $[\mathbf{p}_i, \mathbf{t}_i] = g(\mathcal{N}(v_i), \mathcal{E}_{\mathcal{N}(v_i)} | \theta_g)$, where $\mathbf{p}_i \in \mathbb{R}^n$ and $\mathbf{t}_i \in \mathbb{R}^n$ denote the *source* and *target* embedding of node v_i , respectively, and the embedding dimension n is a hyper-parameter. The source embedding \mathbf{p}_i indicates the attribution of v_i (as a source node) to other nodes, and target embedding is used to compute the attribution of other nodes to this node v_i (as a target node). In this way, the attribution of a source node v_j to a target node can be estimated by an inner product of the source embedding \mathbf{p}_j and target embedding \mathbf{t}_i as follows:

$$\hat{\phi}_{j \rightarrow i} = \langle \mathbf{p}_j, \mathbf{t}_i \rangle, \quad (6)$$

where $\hat{\phi}_{j \rightarrow i}$ is the estimated attribution of source node v_j to target node v_i . Notably, the removal-based attribution is asymmetric according to Equation (5), i.e. $\phi_{j \rightarrow i} \neq \phi_{i \rightarrow j}$, as a result of asymmetrical information flows within the graph structure. Correspondingly, our framework generates different attributions when a node is a source or a target, i.e. $\langle \mathbf{p}_j, \mathbf{t}_i \rangle \neq \langle \mathbf{p}_i, \mathbf{t}_j \rangle$ for $i \neq j$. Likewise, the attribution score of a source node v_j to a target graph/subgraph \mathcal{G} ($v_j \in \mathcal{G}$) can be defined as follows:

$$\hat{\phi}_{j \rightarrow \mathcal{G}} = \langle \mathbf{p}_j, \mathbf{t}_{\mathcal{G}} \rangle, \quad (7)$$

where $\hat{\phi}_{j \rightarrow \mathcal{G}}$ denotes the attribution of node v_j to a target graph \mathcal{G} ; and $\mathbf{t}_{\mathcal{G}} \in \mathbb{R}^n$ is the target embedding of \mathcal{G} , which takes the pooling of target embedding \mathbf{t}_i for nodes $v_i \in \mathcal{G}$.

The parameters of explainer $g(\bullet | \theta_g)$ are trained to learn the removal-based attribution $\phi_{j \rightarrow i}$ introduced in Equation (5) by minimizing the following loss:

$$L = \mathbb{E}_{v_i \sim \mathcal{V}, v_j \sim \mathcal{N}(v_i)} \left[(\hat{\phi}_{j \rightarrow i} - \phi_{j \rightarrow i})^2 \right]. \quad (8)$$

Note that the complexity of Equation (5) is exceedingly high. We incorporate the Monte Carlo estimation of $\phi_{j \rightarrow i}$ as an approximation into Equation (8), which is given as follows:

$$\phi_{j \rightarrow i} \approx \mathbb{E}_{\mathcal{S}_j \sim \mathcal{N}(v_i)} [f(\mathcal{G}_{\mathcal{S}_j}) - f(\mathcal{G}_{\mathcal{N}(v_i) \setminus \mathcal{S}_j})]. \quad (9)$$

Moreover, Equation (9) can be re-formulated into the recursive process as follows,

$$\tilde{\phi}_{j \rightarrow i}^{(t)} = (1 - t^{-1}) \tilde{\phi}_{j \rightarrow i}^{(t-1)} + t^{-1} [f(\mathcal{G}_{\mathcal{S}_j}) - f(\mathcal{G}_{\mathcal{N}(v_i) \setminus \mathcal{S}_j})], \quad (10)$$

where $\mathcal{S}_j \sim \mathcal{N}(v_i)$, $\mathcal{S}_j \ni v_j$ denotes a subset of nodes uniformly sampled from the neighbors $\mathcal{N}(v_i)$; $\tilde{\phi}_{j \rightarrow i}^{(t)}$ denotes the estimation of $\phi_{j \rightarrow i}$ in epoch t ; and its initial value in the first epoch takes $\tilde{\phi}_{j \rightarrow i}^{(0)} = 0$. To this end, the estimation of $\phi_{j \rightarrow i}$ can be integrated with the update of the explainer parameter θ_g into an iterative process, where a hard threshold for subgraph sampling is no longer required.

After the learning of explainer $g(\bullet | \theta_g)$, for each target node v_i or graph \mathcal{G} , the importance of each source node can be generated following the inference process given by Equations (6) or (7), respectively. As our explainer is GNN-based, it can be applied to complex graph structures and generate the attribution for each node in an inductive way, once it is trained.

4.2 Subgraph Sampling

Note that the computational unit (GPU) has limited memory capacity to store the graph during the training. We design a subgraph sampling strategy guided by the training process of the amortized explainer for handling large graph datasets. Specifically, in each iteration, LARA samples a mini-batch of target nodes $\mathcal{V}_t \subseteq \mathcal{V}$. According to the message passing in GNNs, the reception field of a node depends on the number of aggregation layers, which is defined as K . Thus, LARA samples the K -hop neighbors of the target nodes to construct the subgraph $\mathcal{G}_{\tilde{\mathcal{V}}_s}$ to compute the attribution $\tilde{\phi}_{j \rightarrow i}^{(t)}$. Formally, the neighbor samples are given by

$$\tilde{\mathcal{V}}_s = \{v_1, v_2 \mid d(v_1, v_2) \leq K, v_1 \in \mathcal{V}_t, v_2 \in \mathcal{V}\}. \quad (11)$$

After that, LARA samples another subgraph for updating the parameters of the explainer. According to Equation (6), the deduction of explanation-oriented embedding \mathbf{t}_i for $v_i \in \mathcal{V}_s$ requires the K -hop neighbors of the target nodes, so \mathbf{p}_j for $v_j \in \mathcal{N}(v_i)$ requires $2K$ -hop neighbors in total. Therefore, LARA takes a subgraph $\mathcal{G}_{\hat{\mathcal{V}}_s}$ that consists of $2K$ -hop neighbors of the target nodes and the related edges. In this way, the sampled nodes $\hat{\mathcal{V}}_s$ are given by

$$\hat{\mathcal{V}}_s = \{v_1, v_2 \mid d(v_1, v_2) \leq 2K, v_1 \in \mathcal{V}_t, v_2 \in \mathcal{V}\}. \quad (12)$$

The subgraph $\mathcal{G}_{\hat{\mathcal{V}}_s}$ is sampled from the whole graph \mathcal{G} for updating the parameters of the explainer by minimizing the loss in Equation (8).

The training of amortized explainer with subgraph sampling is summarized in Algorithm 1. To be concrete, LARA first samples a subgraph (lines 6-7); then update the estimation of removal-based attribution for the source nodes (line 8); finally update the parameters of the explainer (line 11). The iteration ends with the convergence of the amortized explainer.

Estimation of the Max Hop. The value of K in sampling is directly related to the maximum hop in the message passing. However, in black-box scenarios, we do not know the number of aggregation layers in the target GNN model. A straightforward solution to this problem is to search for the maximum hop neighbors that can disturb the output of the target GNN model.

Concretely, let $\mathcal{G}_{\mathcal{N}_k(v)}$ denote the nodes within the k -hop neighbors of a node v . The maximum hop of the target GNN model is the minimum k that satisfies $f(\mathcal{G}_{\mathcal{N}_{k+1}(v)}) = f(\mathcal{G}_{\mathcal{N}_k(v)})$ as follows,

$$K = \min\{k \mid f(\mathcal{G}_{\mathcal{N}_{k+1}(v)}) = f(\mathcal{G}_{\mathcal{N}_k(v)})\}, \quad (13)$$

where node v can be randomly sampled from the graph. Since a practically deployed GNN model usually cannot have too many aggregation layers to avoid the problem of over-smoothing, the solution of the above problem can be achieved via a grid search over $k = 1, 2, \dots$.

5 Experiment

In this section, we conduct experiments to demonstrate the effectiveness of LARA in explaining node classification and graph classification results. We quantitatively evaluate LARA with respect to interpretation fidelity and throughput in Section 5.1, followed by ablation study and hyper-parameter analysis for LARA. Section 5.3 demonstrates several case studies on node and graph classification.

5.1 Quantitative Evaluation

We evaluate the faithfulness and efficiency of LARA compared to state-of-the-art methods: GNNExplainer [36], PGExplainer [24], GraphSVX [9] and OrphicX [19]. The experiments are conducted on six benchmark datasets: BA-Shapes, BA-Community, Tree-Cycles [36] and ogbn-arxiv [14] for node classification, and BA-2Motifs [24] and MUTAG [7] for graph classification. More details about the implementation, datasets, baseline methods, and hyper-parameter settings are given in Appendix D.

Algorithm 1 Training of Explainer $g(\bullet \mid \theta_g^*)$.

- 1: **Input:** Graph $\mathcal{G}(\mathcal{V}, \mathcal{E})$, target GNN model $f(\cdot)$.
 - 2: **Output:** Explainer $g(\bullet \mid \theta_g^*)$.
 - 3: Initialize $\tilde{\phi}_{j \rightarrow i}^{(0)} = 0$ for $v_i, v_j \in \mathcal{G}$. Set $t = 1$
 - 4: **while** *not converge* **do**
 - 5: # Estimate the removal-based attribution.
 - 6: Sample a mini-batch of target nodes $\mathcal{V}_t \subseteq \mathcal{V}$.
 - 7: Sample a subgraph following Equation (11).
 - 8: Update $\tilde{\phi}_{j \rightarrow i}^{(t)}$ following Equation (10).
 - 9: # Update explainer parameters.
 - 10: Sample a subgraph following Equation (12).
 - 11: Update the parameters of $g(\bullet \mid \theta_g)$ by

$$\theta_g^* = \arg \min_{\theta} \mathbb{E}_{v_i \sim \mathcal{V}_t, v_j \sim \mathcal{N}(v_i)} [(\hat{\phi}_{j \rightarrow i} - \tilde{\phi}_{j \rightarrow i}^{(t)})^2]$$
 - 12: $t = t + 1$
 - 13: **end while**
-

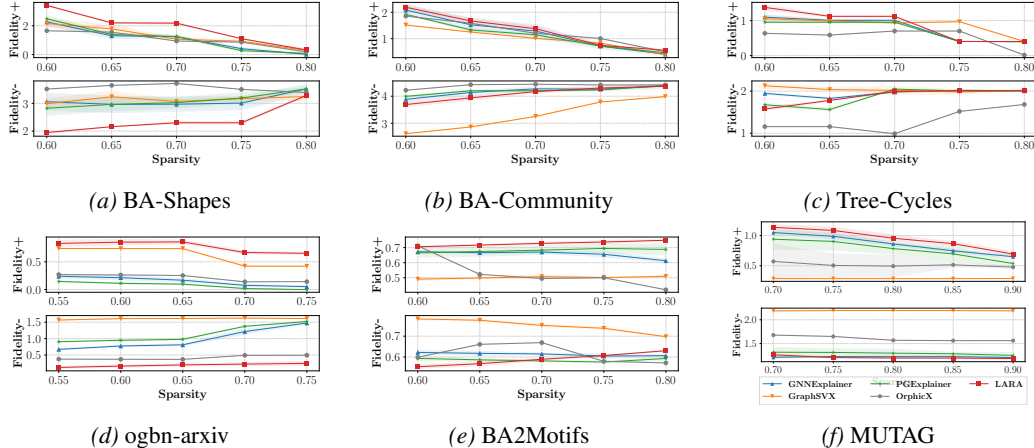


Figure 4: Interpretation fidelity versus sparsity of neighbors on (a) BA-Shape, (b) BA-Community, (c) Tree-Cycles, (d) ogbn-arxiv, (e) BA2Motifs, and (f) MUTAG datasets. In sub-figures of Fidelity⁺, a line placed above indicates better performance. In sub-figures of Fidelity⁻, a line placed below indicates better performance.

Table 1: Throughput of LARA compared with state-of-the-art methods. Results are shown in (mean \pm std) over five runs and the best results are marked in bold.

	Method	BA-Shapes	BA-Community	Tree-Cycles	BA-2Motifs	MUTAG	ogbn-arxiv
Throughput \uparrow	GNNExplainer	3.15 \pm 0.11	2.19 \pm 0.09	4.18 \pm 0.03	6.05 \pm 0.02	15.38 \pm 0.63	9.35 \pm 0.06
	GraphSVX	9.51 \pm 0.04	10.58 \pm 0.67	10.31 \pm 0.19	4.90 \pm 0.18	2.09 \pm 0.21	0.95 \pm 0.06
	PGExplainer	22.95 \pm 0.14	13.67 \pm 0.18	423.78 \pm 4.51	490.55 \pm 9.94	80.39 \pm 2.53	28.38 \pm 0.07
	OrphicX	262.49 \pm 7.95	196.23 \pm 3.39	447.39 \pm 5.10	373.21 \pm 5.12	286.07 \pm 3.07	77.85 \pm 0.07
	LARA	670.54 \pm 1.94	644.63 \pm 1.03	674.12 \pm 4.06	635.10 \pm 7.24	334.44 \pm 2.18	237.97 \pm 3.87

Fidelity. Figure 4 shows the Fidelity⁺ and Fidelity⁻ versus the sparsity of neighbors¹, where LARA is compared with state-of-the-art baseline methods on the six benchmark datasets. Overall, LARA (in red) outperforms baseline methods on most of the datasets in terms of higher Fidelity⁺ and lower Fidelity⁻, particularly on the large graph dataset ogbn-arxiv, as shown in Figure 4 (d). This highlights its potential in faithful explanations for real-world use cases. Among the baseline methods, GNNExplainer, PGExplainer and OrphicX adopt the MI value for node attribution, which is less effective than LARA, especially on ogbn-arxiv. This is consistent with our observations in Section 3, demonstrating the advantage of LARA towards maximizing the interpretation fidelity by learning our proposed removal-based attribution.

Efficiency. According to Table 1, LARA shows a significant improvement in throughput on all datasets compared with baseline methods. As a non-amortized method, GNNExplainer shows a considerably lower throughput of interpretation than other methods, because it has to learn an explainer for each instance. GraphSVX relies on solving a matrix equation to estimate the importance of each neighbor. This is separately conducted for each target node, resulting in considerably low efficiency. Although PGExplainer and OrphicX can simultaneously generate a batch of explanations, their time complexity increases with the edge number contained in the relevant subgraph of the target node. As an amortized method, LARA has a constant time complexity of the explanation based on a feed-forward process of the explainer, and can efficiently explain multiple nodes within a batch.

Scalability. We study the scalability of LARA on a large graph ogbn-arxiv. The time latency of explaining different numbers of nodes from the ogbn-arxiv are listed in Table 3. In particular, as the node number grows from 10^2 to 10^5 , GNNExplainer and PGExplainer show approximate 12000s and 3500s growth of time latency (Δ time latency), respectively. In contrast, LARA has only 400s growing, which shows stronger scalability than baseline methods. Moreover, LARA exhibits about 90% less time latency compared to the competitive baseline PGExplainer in general. The result demonstrates the potential of LARA in real-world applications such as in a social network with millions of nodes and edges.

¹In the experiment of Fidelity⁺, a sparsity of $p\%$ indicates top $(1 - p\%)$ important neighbors are removed; in the experiment of Fidelity⁻, a sparsity of $p\%$ indicates the least important $p\%$ neighbors are removed, following the definition in [38].

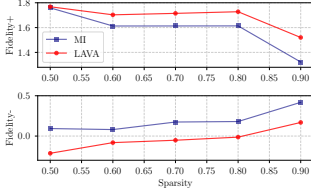


Figure 5: LARA v.s. learning MI.

Table 2: LARA v.s. single-embedding baseline method.

	Method	Tree-Cycles	ogbn-arxiv	BA-2Motif	MUTAG
Fidelity ⁺ ↑	Single	1.61	1.18	0.60	1.31
	LARA	2.19	1.54	0.65	1.36
Fidelity ⁻ ↓	Single	1.23	0.16	0.58	1.24
	LARA	1.02	0.02	0.55	1.20

Table 3: Time latency (s) on ogbn-arxiv.

Node #	10 ²	10 ³	10 ⁴	10 ⁵
GNNExplainer	15.34	119.84	1186.43	12101.1
PGExplainer	5.63	35.52	490.48	3534.65
LARA	0.54	4.23	39.92	416.50

Table 4: Effectiveness of explainer layer number.

Aggr. Layer	0	1	2	3	4
Fidelity ⁺ ↑	3.46	3.25	3.68	3.72	3.53
Fidelity ⁻ ↓	2.34	2.52	2.52	2.32	2.39
Throughput	3308.77	1530.98	903.30	645.93	499.71

5.2 Ablation Study and Hyper-parameter Analysis

In the ablation study, we validate the effectiveness of key components in the LARA framework: 1) learning the removal-based attribution; 2) bidirectional embedding (source and target embeddings are learned separately). After this, we study the interpretation fidelity affected by the key hyper-parameter of LARA, i.e., the number of aggregation layers in the amortized explainer.

Learning Removal- v.s. MI-based Attribution. We demonstrate the advantage of learning removal-based attribution in LARA by comparing it with the baseline method that learns MI-based attribution. The baseline follows existing work [36, 24] to adopt the mutual information for the supervision of training the explainer. Specifically, the parameters of amortized explainer are updated to minimize the loss function given by $L = \mathbb{E}_{v_i \sim \mathcal{V}, v_j \sim \mathcal{N}(v_i)} [\hat{\phi}_{j \rightarrow i} - I(v_j; \hat{y})]^2$, where the MI value is given by $I(v_j; \hat{y}) = -\mathbb{E}_{y \sim f(\mathcal{G}_{\mathcal{N}(v_i)}, \mathcal{S}_j \sim \mathcal{N}(v_i))} \log \frac{p(\hat{y}=y | \mathcal{G}_{\mathcal{N}(v_i)})}{p(\hat{y}=y | \mathcal{G}_{\mathcal{S}_j})}$. The experiment is conducted on the ogbn-arxiv dataset (a real-world large graph), and the implementation details can be found in Appendix D. Figure 5 shows the interpretation fidelity of LARA compared to the baseline method, where LARA consistently outperforms the baseline method. This is consistent with our observation in Section 3, highlighting the advantage of our proposed removal-based attribution in generating faithful GNN explanations and serving as the objective function for training the amortized explainer.

Effectiveness of Bidirectional Embedding. We demonstrate the advantage of LARA by learning the source and target embedding separately in Equation (6). In contrast, a baseline method is to learn a single embedding \mathbf{t} by the explainer to estimate the node attribution. Concretely, the attribution of a node v_j to another node v_i is given by $\hat{\phi}_{j \rightarrow i} = \langle \mathbf{t}_j, \mathbf{t}_i \rangle$. In this case, $\hat{\phi}_{i \rightarrow j} = \hat{\phi}_{j \rightarrow i}$, and its attribution to a graph \mathcal{G} is estimated based on the pooling of \mathbf{t}_i for $v_i \in \mathcal{G}$. Table 2 compares the fidelity of LARA versus the baseline on both node classification and graph classification tasks: the Tree-Cycles, ogbn-arxiv, BA-2Motif, and MUTAG datasets. It is observed that LARA consistently outperforms the baseline. In particular, in node classification, LARA shows a 0.58 improvement in Fidelity⁺, and a 0.15 reduction in Fidelity⁻. This emphasizes the advantage and necessity of LARA in learning the source and target embedding separately for each node to achieve faithful explanations.

Explainer with Different Numbers of Layers. We study the performance of LARA affected by the number of aggregation layers in the amortized explainer $g(\bullet | \theta_g)$. Table 4 lists the fidelity of LARA with respect to different numbers of aggregation layers in the amortized explainer, where the explainer without aggregation is essentially a multi-layer perceptron (MLP) model. It is observed that the GNN-based explainer (#AggrLayer = 3) achieves the highest fidelity. The performance on fidelity metrics increases with the number of aggregation layers, suggesting that the node information aggregation in the framework of LARA benefits the training of amortized explainer. Nevertheless, too many layers (#AggrLayer > 3) could result in redundancy and thus hurt the performance. Moreover, an inspiring observation is that LARA has moderate performance in fidelity without node information aggregation, where Fidelity⁺ = 3.46 and Fidelity⁻ = 2.34. This indicates the effectiveness of LARA even without a GNN-based explainer. Notably, since an MLP-based explainer enables a significant improvement in throughput, implementing LARA with an MLP-based explainer highlights a potential solution for industrial applications.

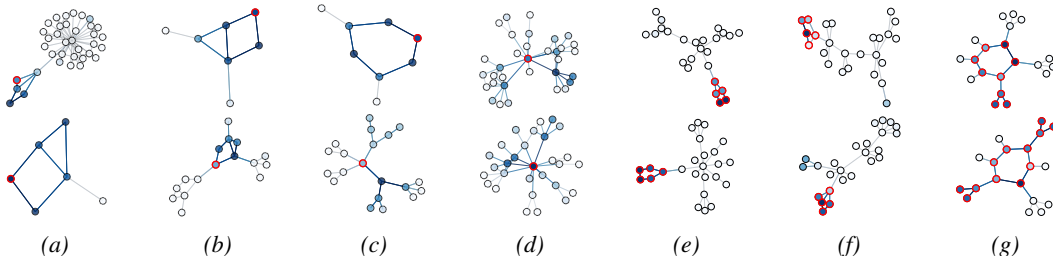


Figure 6: Qualitative results of node and graph classification. **Node classification:** (a) BA-Shapes (b) BA-Community (c) Tree-Cycles (d) ogbn-arxiv; **Graph classification** (e) BA-2Motifs, Pentagon (f) BA-2Motifs, House (g) MUTAG, Mutagen. For node classification, darker nodes refer to more important nodes for the prediction of the target node (to be explained and highlighted in red color) in (a)(b)(c)(d). For graph classification, darker nodes indicate more important nodes for the classification, and red nodes indicate the ground truth motif in (e)(f)(g).

5.3 Qualitative Results

In this section, we visualize the explanations generated by LARA, demonstrating its power in helping human users understand GNN models. The explanation of node classification is shown in Figure 6 (a)-(d), where the target node is highlighted in red, and the dark blue nodes indicate important neighbors suggested by LARA. The explanation of graph classification is shown in Figure 6 (e)-(g), where the ground truth explanation is marked in red, and the recognized important nodes are in dark blue.

Node Classification. The classification task aims to predict whether a target node belongs to a specific structural subgraph on the BA-shapes and Tree-Cycles datasets, or a community on the BA-Community dataset. According to the explanation given by LARA in Figure 6 (a)-(d), the important neighbors for the target nodes fall into a local subgraph with a specific structure. e.g. a motif of “house” on the BA-shapes and BA-Community datasets, a hexagon or tree structures on Tree-Cycles. Such faithful and intuitive explanations are essential to increase user trust in practical use cases. Different phenomena can be observed on the ogbn-arxiv dataset as demonstrated in Figure 6 (d), where no ground truth pattern is available. Concretely, the direct neighbors have more contribution in the prediction of the target node than the non-adjacent nodes. On the ogbn-arxiv dataset, each node represents a paper, each edge indicates a citation of another one, and the classification aims to predict whether a paper belongs to one of the 40 arXiv CS subject areas. As common sense, the papers cited with each other likely belong to the same subject area. Explanations in Figure 6 (d) reflect the intuition of this task, indicating the effectiveness of LARA.

Graph Classification. The graph classification aims to detect whether a graph has a specific subgraph. According to the ground truth explanation, the key subgraph structure for the classification is a pentagon or a house structure on the BA-2Motifs dataset. Notably, the nodes on the edge inside the house are the most important ones as highlighted in Figure 6 (f). On MUTAG, the ground truth for the class mutagen is a hexagon (known as a “carbon ring”) with a three-node (NH_2/NO_2) group, which is recognized by LARA in Figure 6 (g). As shown in Figure 6 (e)(f)(g), LARA successfully generates explanations of each graph consistent with the ground truth. The results validate the capability of LARA in explaining graph classification.

6 Conclusion

In this work, we propose LARA for efficient and faithful GNN explanations. Specifically, we introduce a removal-based attribution approach, which outperforms the mutual information as guidance of generating faithful explanations, especially on large graphs. The correlation between removal-based attribution and interpretation fidelity is theoretically and experimentally validated. Following this direction, LARA trains an amortized explainer to maximize fidelity and incorporates a subgraph sampling strategy for scalability on large graphs. After training, LARA generates batch-wise node explanations efficiently in a feed-forward process. Experimental results demonstrate LARA can significantly improve the efficiency and scalability of GNN explanations, while keeping competitive interpretation fidelity. This highlights the potential of LARA being applied to the large-scale social graphs with millions of nodes and edges in real-world scenarios.

References

- [1] David Alvarez Melis and Tommi Jaakkola. Towards robust interpretability with self-explaining neural networks. *Advances in neural information processing systems*, 31, 2018.
- [2] Albert-László Barabási and Réka Albert. Emergence of scaling in random networks. *science*, 286(5439):509–512, 1999.
- [3] Jianbo Chen, Le Song, Martin Wainwright, and Michael Jordan. Learning to explain: An information-theoretic perspective on model interpretation. In *International Conference on Machine Learning*, pages 883–892. PMLR, 2018.
- [4] Yu-Neng Chuang, Guanchu Wang, Fan Yang, Xuanting Cai, Tripathi Pushkar, and Xia Hu. CoRTX: Contrastive framework for real-time explanation. In *Submitted to The Eleventh International Conference on Learning Representations*, 2023. URL <https://openreview.net/forum?id=L2MU0Up0beo>. under review.
- [5] Yu-Neng Chuang, Guanchu Wang, Fan Yang, Zirui Liu, Xuanting Cai, Mengnan Du, and Xia Hu. Efficient xai techniques: A taxonomic survey. *arXiv preprint arXiv:2302.03225*, 2023.
- [6] Ian Covert, Scott M Lundberg, and Su-In Lee. Explaining by removing: A unified framework for model explanation. *J. Mach. Learn. Res.*, 22:209–1, 2021.
- [7] Asim Kumar Debnath, Rosa L Lopez de Compadre, Gargi Debnath, Alan J Shusterman, and Corwin Hansch. Structure-activity relationship of mutagenic aromatic and heteroaromatic nitro compounds. correlation with molecular orbital energies and hydrophobicity. *Journal of medicinal chemistry*, 34(2):786–797, 1991.
- [8] Keyu Duan, Zirui Liu, Peihao Wang, Wenqing Zheng, Kaixiong Zhou, Tianlong Chen, Xia Hu, and Zhangyang Wang. A comprehensive study on large-scale graph training: Benchmarking and rethinking. *arXiv preprint arXiv:2210.07494*, 2022.
- [9] Alexandre Duval and Fragkiskos D Malliaros. Graphsvx: Shapley value explanations for graph neural networks. In *Joint European Conference on Machine Learning and Knowledge Discovery in Databases*, pages 302–318. Springer, 2021.
- [10] Wenqi Fan, Yao Ma, Qing Li, Yuan He, Eric Zhao, Jiliang Tang, and Dawei Yin. Graph neural networks for social recommendation. In *The world wide web conference*, pages 417–426, 2019.
- [11] Qizhang Feng, Ninghao Liu, Fan Yang, Ruixiang Tang, Mengnan Du, and Xia Hu. Degree: Decomposition based explanation for graph neural networks. In *International Conference on Learning Representations*, 2021.
- [12] Thorben Funke, Megha Khosla, and Avishek Anand. Hard masking for explaining graph neural networks. 2020.
- [13] EU GDPR. Recital 71, 2016. URL <https://www.privacy-regulation.eu/en/r71.htm>.
- [14] Weihua Hu, Matthias Fey, Marinka Zitnik, Yuxiao Dong, Hongyu Ren, Bowen Liu, Michele Catasta, and Jure Leskovec. Open graph benchmark: Datasets for machine learning on graphs. *Advances in neural information processing systems*, 33:22118–22133, 2020.
- [15] Qiang Huang, Makoto Yamada, Yuan Tian, Dinesh Singh, and Yi Chang. Graphlime: Local interpretable model explanations for graph neural networks. *IEEE Transactions on Knowledge and Data Engineering*, 2022.
- [16] Neil Jethani, Mukund Sudarshan, Yindalon Aphinyanaphongs, and Rajesh Ranganath. Have we learned to explain?: How interpretability methods can learn to encode predictions in their interpretations. In *International Conference on Artificial Intelligence and Statistics*, pages 1459–1467. PMLR, 2021.
- [17] Neil Jethani, Mukund Sudarshan, Ian Connick Covert, Su-In Lee, and Rajesh Ranganath. Fastshap: Real-time shapley value estimation. In *International Conference on Learning Representations*, 2021.

- [18] Wanyu Lin, Hao Lan, and Baochun Li. Generative causal explanations for graph neural networks. In *International Conference on Machine Learning*, pages 6666–6679. PMLR, 2021.
- [19] Wanyu Lin, Hao Lan, Hao Wang, and Baochun Li. Orphicx: A causality-inspired latent variable model for interpreting graph neural networks. In *Proceedings of the IEEE/CVF Conference on Computer Vision and Pattern Recognition*, pages 13729–13738, 2022.
- [20] Ninghao Liu, Qizhang Feng, and Xia Hu. Interpretability in graph neural networks. *Graph Neural Networks: Foundations, Frontiers, and Applications*, pages 121–147, 2022.
- [21] Zirui Liu, Shengyuan Chen, Kaixiong Zhou, Daochen Zha, Xiao Huang, and Xia Hu. Rsc: Accelerating graph neural networks training via randomized sparse computations. *arXiv preprint arXiv:2210.10737*, 2022.
- [22] Zirui Liu, Kaixiong Zhou, Fan Yang, Li Li, Rui Chen, and Xia Hu. EXACT: Scalable graph neural networks training via extreme activation compression. In *International Conference on Learning Representations*, 2022. URL https://openreview.net/forum?id=vkaMaq95_rX.
- [23] Scott M Lundberg and Su-In Lee. A unified approach to interpreting model predictions. *Advances in neural information processing systems*, 30, 2017.
- [24] Dongsheng Luo, Wei Cheng, Dongkuan Xu, Wenchao Yu, Bo Zong, Haifeng Chen, and Xiang Zhang. Parameterized explainer for graph neural network. *Advances in neural information processing systems*, 33:19620–19631, 2020.
- [25] Tomas Mikolov, Ilya Sutskever, Kai Chen, Greg S Corrado, and Jeff Dean. Distributed representations of words and phrases and their compositionality. *Advances in neural information processing systems*, 26, 2013.
- [26] Phillip E Pope, Soheil Kolouri, Mohammad Rostami, Charles E Martin, and Heiko Hoffmann. Explainability methods for graph convolutional neural networks. In *Proceedings of the IEEE/CVF Conference on Computer Vision and Pattern Recognition*, pages 10772–10781, 2019.
- [27] Yao Rong, Tobias Leemann, Vadim Borisov, Gjergji Kasneci, and Enkelejda Kasneci. A consistent and efficient evaluation strategy for attribution methods. *arXiv preprint arXiv:2202.00449*, 2022.
- [28] Thomas Schnake, Oliver Eberle, Jonas Lederer, Shinichi Nakajima, Kristof T Schütt, Klaus-Robert Müller, and Grégoire Montavon. Higher-order explanations of graph neural networks via relevant walks. *IEEE transactions on pattern analysis and machine intelligence*, 44(11): 7581–7596, 2021.
- [29] Richard Tomsett, Dan Harborne, Supriyo Chakraborty, Prudhvi Gurram, and Alun Preece. Sanity checks for saliency metrics. In *Proceedings of the AAAI conference on artificial intelligence*, volume 34, pages 6021–6029, 2020.
- [30] Minh Vu and My T Thai. Pgm-explainer: Probabilistic graphical model explanations for graph neural networks. *Advances in neural information processing systems*, 33:12225–12235, 2020.
- [31] Guanchu Wang, Yu-Neng Chuang, Mengnan Du, Fan Yang, Quan Zhou, Pushkar Tripathi, Xuanting Cai, and Xia Hu. Accelerating shapley explanation via contributive cooperater selection. In *International Conference on Machine Learning*, pages 22576–22590. PMLR, 2022.
- [32] Shiwen Wu, Fei Sun, Wentao Zhang, Xu Xie, and Bin Cui. Graph neural networks in recommender systems: a survey. *ACM Computing Surveys*, 55(5):1–37, 2022.
- [33] Zonghan Wu, Shirui Pan, Fengwen Chen, Guodong Long, Chengqi Zhang, and S Yu Philip. A comprehensive survey on graph neural networks. *IEEE transactions on neural networks and learning systems*, 32(1):4–24, 2020.

- [34] Makoto Yamada, Wittawat Jitkrittum, Leonid Sigal, Eric P Xing, and Masashi Sugiyama. High-dimensional feature selection by feature-wise kernelized lasso. *Neural computation*, 26(1): 185–207, 2014.
- [35] Chih-Kuan Yeh, Cheng-Yu Hsieh, Arun Suggala, David I Inouye, and Pradeep K Ravikumar. On the (in) fidelity and sensitivity of explanations. *Advances in Neural Information Processing Systems*, 32, 2019.
- [36] Zhitao Ying, Dylan Bourgeois, Jiaxuan You, Marinka Zitnik, and Jure Leskovec. Gnnexplainer: Generating explanations for graph neural networks. *Advances in neural information processing systems*, 32, 2019.
- [37] Hao Yuan, Haiyang Yu, Jie Wang, Kang Li, and Shuiwang Ji. On explainability of graph neural networks via subgraph explorations. In *International Conference on Machine Learning*, pages 12241–12252. PMLR, 2021.
- [38] Hao Yuan, Haiyang Yu, Shurui Gui, and Shuiwang Ji. Explainability in graph neural networks: A taxonomic survey. *IEEE Transactions on Pattern Analysis and Machine Intelligence*, 2022.
- [39] Hanqing Zeng, Hongkuan Zhou, Ajitesh Srivastava, Rajgopal Kannan, and Viktor Prasanna. Graphsaint: Graph sampling based inductive learning method. *arXiv preprint arXiv:1907.04931*, 2019.
- [40] Shichang Zhang, Yozen Liu, Neil Shah, and Yizhou Sun. Gstarx: Explaining graph neural networks with structure-aware cooperative games. In *Advances in Neural Information Processing Systems*, 2022.
- [41] Yue Zhang, David Defazio, and Arti Ramesh. Relex: A model-agnostic relational model explainer. In *Proceedings of the 2021 AAAI/ACM Conference on AI, Ethics, and Society*, pages 1042–1049, 2021.

A Experimental Details in Section 3

In this section, we provide implementation details of the experiment in Section 3. In order to validate the correlation between MI- or removal-based attribution value and the fidelity score, we randomly sample a subset of neighbor nodes $\mathcal{J} \subseteq \mathcal{N}(v_i)$ of a target node v_i as the explanatory nodes (important nodes to the model prediction). Then, we calculate the MI- or removal-based attribution value of \mathcal{J} to the original prediction for the target node $f(\mathcal{G}_{\mathcal{N}(v_i)})$ following previous work [36]. Similar to Definition 3.2, we denote the MI value of a subset \mathcal{J} to a target node v_i as $\alpha_{\mathcal{J} \rightarrow i}$. Likewise, removal-based attribution of the subset \mathcal{J} to v_i is denoted as $\phi_{\mathcal{J} \rightarrow i}$. Concretely, we calculate the MI value $\alpha_{\mathcal{J} \rightarrow i}$ as follows:

$$\alpha_{\mathcal{J} \rightarrow i} = -\mathbb{E}_{y \sim f(\mathcal{G}_{\mathcal{N}(v_i)})} p(\hat{y} = y | \mathcal{G}_{\mathcal{N}(v_i)}) \log p(\hat{y} = y | \mathcal{G}_{\mathcal{J}}). \quad (14)$$

For the same \mathcal{J} , we calculate the removal-based attribution score as:

$$\phi_{\mathcal{J} \rightarrow i} = \mathbb{E}_{j \sim \mathcal{J}} [f(\mathcal{G}_{v_j}) - f(\mathcal{G}_{\mathcal{N}(v_i) \setminus v_j})]. \quad (15)$$

For each subfigure in Figure 2 in Section 3, we randomly sample one hundred input pairs (\mathcal{J}, v_i) to calculate the MI or removal-based attribution values, which are plotted on the x-axis.

Given (\mathcal{J}, v_i) , Fidelity⁺ is calculated as follows:

$$\text{Fidelity}^+(v_i, \mathcal{J}) = \mathcal{G}_{\mathcal{N}(v_i)} - f(\mathcal{G}_{\mathcal{N}(v_i) \setminus \mathcal{J}}), \quad (16)$$

which is plotted on the y-axis. For Figure 2 (a), we use the dataset BA-Community to conduct the experiment, while ogbn-arxiv is used in Figure 2 (b) and Figure 2 (c).

B Proof of Theorem 3.1

In this section, we provide the proof of Theorem 3.1.

Proof. We take $\phi_{j \rightarrow i} = \mathbb{E}_{\mathcal{S}_j \subseteq \mathcal{N}(v_i)} [f(\mathcal{G}_{\mathcal{S}_j}) - f(\mathcal{G}_{\mathcal{N}(v_i) \setminus \mathcal{S}_j})]$ into $\mathbb{E}_{j \sim \mathcal{J}} \phi_{j \rightarrow i}$,

$$\mathbb{E}_{j \sim \mathcal{J}} \mathbb{E}_{\mathcal{S}_j \subseteq \mathcal{N}(v_i)} [f(\mathcal{G}_{\mathcal{S}_j}) - f(\mathcal{G}_{\mathcal{N}(v_i) \setminus \mathcal{S}_j})] \quad (17)$$

$$= \mathbb{E}_{j \sim \mathcal{J}} \mathbb{E}_{\mathcal{S}_j \subseteq \mathcal{N}(v_i)} \left[\underbrace{(f(\mathcal{G}_{\mathcal{N}(v_i)}) - f(\mathcal{G}_{\mathcal{N}(v_i) \setminus \mathcal{S}_j}))}_{\text{Fidelity}^+(v_i, \mathcal{S}_j)} - \underbrace{(f(\mathcal{G}_{\mathcal{N}(v_i)}) - f(\mathcal{G}_{\mathcal{S}_j}))}_{\text{Fidelity}^-(v_i, \mathcal{S}_j)} \right] \quad (18)$$

$$= \mathbb{E}_{j \sim \mathcal{J}} \mathbb{E}_{\mathcal{S}_j \subseteq \mathcal{N}(v_i)} [\Delta \text{Fidelity}(v_i, \mathcal{S}_j)]. \quad (19)$$

Likewise, we get

$$\mathbb{E}_{j \sim \mathcal{J}^*} \mathbb{E}_{\mathcal{S}_j \subseteq \mathcal{N}(v_i)} [f(\mathcal{G}_{\mathcal{S}_j}) - f(\mathcal{G}_{\mathcal{N}(v_i) \setminus \mathcal{S}_j})] \quad (20)$$

$$= \mathbb{E}_{j \sim \mathcal{J}^*} \mathbb{E}_{\mathcal{S}_j \subseteq \mathcal{N}(v_i)} [\Delta \text{Fidelity}(v_i, \mathcal{S}_j)]. \quad (21)$$

Since $\mathbb{E}_{j \sim \mathcal{J}} \phi_{j \rightarrow i} \leq \mathbb{E}_{j \sim \mathcal{J}^*} \phi_{j \rightarrow i}$, we get

$$\mathbb{E}_{j \sim \mathcal{J}} \mathbb{E}_{\mathcal{S}_j \subseteq \mathcal{N}(v_i)} [f(\mathcal{G}_{\mathcal{S}_j}) - f(\mathcal{G}_{\mathcal{N}(v_i) \setminus \mathcal{S}_j})] \leq \mathbb{E}_{j \sim \mathcal{J}^*} \mathbb{E}_{\mathcal{S}_j \subseteq \mathcal{N}(v_i)} [f(\mathcal{G}_{\mathcal{S}_j}) - f(\mathcal{G}_{\mathcal{N}(v_i) \setminus \mathcal{S}_j})] \quad (22)$$

$$\mathbb{E}_{j \sim \mathcal{J}} \mathbb{E}_{\mathcal{S}_j \subseteq \mathcal{N}(v_i)} [\Delta \text{Fidelity}(v_i, \mathcal{S}_j)] \leq \mathbb{E}_{j \sim \mathcal{J}^*} \mathbb{E}_{\mathcal{S}_j \subseteq \mathcal{N}(v_i)} [\Delta \text{Fidelity}(v_i, \mathcal{S}_j)]. \quad (23)$$

□

C Experimental Details of Figure 1

We plot Fidelity⁺ and throughput in the radar figure for four baselines and our method. Fidelity⁺ is the averaged value over different sparsity given in Figure 4 (subgraphs of Fidelity⁺) in Section 5.1. The throughput in the plot is given in Table 1 in Section 5.1.

D Experimental Details in Section 5

In this section, we introduce details about the used datasets, target models, baseline models, hyperparameter settings, implementation details of experiments in Section 5.2, and used computational infrastructure for our experiments.

Table 5: Dataset details. The upper part contains the node classification task and the bottom part is graph classification.

	#graphs	#nodes	#edges	#labels	node feature dim
BA-Shapes	1	700	4,110	4	10
BA-Community	1	1,400	8,920	8	10
Tree-Cycles	1	871	1,950	2	10
ogbn-arxiv	1	169,343	1,166,243	40	128
BA-2Motifs	1,000	25,000	51,392	2	10
MUTAG	4,377	131,488	266,894	2	14

D.1 Datasets

We deploy LARA to explain node classification on BA-Shapes, BA-Community, Tree-Cycles and ogbn-arxiv; and graph classification on the BA-2Motifs and MUTAG datasets. In particular, the BA-Shapes dataset contains a 300-node Barabási-Albert (BA) graph [2] with 80 five-node “house” motifs randomly attached to it. Each node has a label out of four according to the position in the motif. The BA-Community dataset consists of two BA-Shapes datasets with random edges connecting them, including eight classes. The Tree-Cycles dataset has two node classes indicating whether a node belongs to a base graph (eight-level balanced binary tree) or a motif (six-node cycle). The BA-2Motifs has 1,000 synthetic graphs with binary labels, while MUTAG contains 4,337 molecule graphs with binary labels. The statistics of each dataset can be found in Table 5. For all datasets, the split of training/validation/test set is 80%/10%/10%.

Ground truth motifs on synthesis datasets and MUTAG are listed in Figure 7. On BA-Shapes and BA-Community, the labels of nodes are decided by the position of the node in the “house” motif, while on Tree-Cycles the label of nodes is dependent whether the node is inside the six-node cycle or on the tree structure. On BA-2Motifs, the graph is classified by the type of motifs. In MUTAG, there are two different classes: mutagen and non-mutagen. If there is a pattern of NH_2/NO_2 together with the carbon ring, then this graph belongs to the class mutagen, otherwise to the class Non-mutagen.

To the best of our knowledge, this is the first work to benchmark the explanations on large graph datasets like ogbn-arxiv [14]. The ogbn-arxiv dataset is essentially a citation network, containing a total of 169,343 nodes and 1,166,243 edges, where a node represents a paper and an edge indicates a citation of one paper by another one. Each node is encoded in a 128-dim feature vector provided by the Word2Vec model with the MAG corpus [25]. On this dataset, the target GNN model is trained to classify a paper into one of the 40 arXiv CS subject areas.

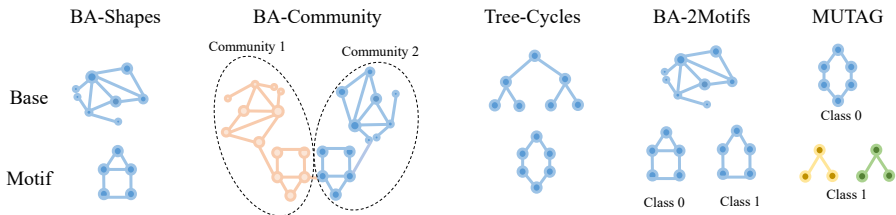


Figure 7: Ground truth motif on BA-Shapes, BA-Community, Tree-Cycles (node classification datasets), BA-2Motif and MUTAG (graph classification datasets).

D.2 Target Model Details

For each dataset, we use the target model under the settings as given in [24] for BA-Shapes, BA-Community, Tree-Cycles, BA-2Motifs and MUTAG ². For each of these datasets, a GCN model containing three layers is trained. In the graph classification models, a max-pooling layer is inserted to get the graph embedding before the final fully-connected layer. On ogbn-arxiv, we train a GraphSAINT [39] model with two layers using a subgraph-wise sampling strategy following the

²We use the trained target models at <https://github.com/LarsHoldijk/RE-ParameterizedExplainerForGraphNeuralNetworks>.

settings in [8]³. For the synthetic datasets, we use the same splits provided in [24]. For MUTAG and ogbn-arxiv, we use their original splits. On all datasets, we use the identical target model as well as the same data split for GNNExplainer, PGExplainer, GraphSVX, OrphicX and LARA to conduct a fair comparison of their interpretation.

Table 6 lists the accuracy of the target models on different splits on each dataset.

	BA-Shapes	BA-Community	Tree-Cycles	ogbn-arxiv	BA-2Motifs	MUTAG
Training	0.97	0.90	0.94	0.56	1.0	0.82
Validation	1.00	0.76	0.98	0.56	1.0	0.82
Test	1.00	0.72	0.94	0.50	1.00	0.81

Table 6: Accuracy of target models.

D.3 Baseline Methods

We introduce in this section the used state-of-the-art baseline methods in comparison to our proposed framework LARA. **GNNExplainer** [36] explains predictions via soft masks for edges and node features, which maximizes the mutual information between the predictions of original graphs and the newly generated ones. For each instance, a soft mask needs to be learned. **GraphSVX** [9] also provides local explanations. The authors propose to estimate Shapley values for nodes (and features on a node) adopted kernel SHAP [23] and use SHAP values as model explanations. **PGExplainer** [24] learns a model using the reparameterization trick to predict edge masks indicating their importance, while **OrphicX** [19] identifies the causal factors by maximizing the information flow from the latent features to the model predictions, which are used to produce explanations. All methods estimate the explanation of a node by averaging the importance scores of the edges connected to the node, if the original method is designed for explaining through edge importance. We adopt code and follow their hyper-parameter settings for training the explainer given in the official code for baseline methods. For GraphSVX, we deploy the uniform mask sampling for estimating SHAP values⁴.

D.4 Hyper-parameter Settings

We adopt a GCN-based model to build the explainer $g(\bullet | \theta_g^*)$. The number of aggregation layers in the explainer is set to the Max Hop value defined in Section 4.2. For the explanation of graph classification, the target embedding t_G takes the max-pooling of the target embeddings t_j for nodes $v_j \in \mathcal{G}$. The explainer is trained with the default splitting of the training/validation/testing sets on each dataset. To update the parameters of $g(\bullet | \theta_g^*)$, we deploy the Adam optimizer with a 10^{-3} learning rate for node classification and a 10^{-4} learning rate for graph classification. The mini-batch size of sampling target nodes is set to 64 for all datasets.

D.5 Fidelity Average

Table 2 and 4 in Section 5.2 report the averaged fidelity values. We first calculate Fidelity⁺ and Fidelity⁻ at different sparsity (see Figure 4) and then use the averaged value to represent the final fidelity in these tables. We take a wide range of sparsity (from 0.3 to 0.7 with a step size of 0.1) in these two experiments. Following [38], the sparsity of a given node v_i is defined as:

$$\text{Sparsity}(v_i, \mathcal{N}_{v_i}^*) = 1 - \frac{|\mathcal{N}_{v_i}^*|}{|\mathcal{N}(v_i)|}, \quad (24)$$

where $\mathcal{N}_{v_i}^*$ is the set of important neighbor nodes given by the explanation. In Fidelity⁺, the node set $\mathcal{N}_{v_i}^*$ is removed, while in Fidelity⁻, $\mathcal{N}_{v_i}^*$ is kept but the rest nodes are removed. A higher sparsity is desired for an explanation since it captures sufficiently important information in a small subset of nodes. Through different sparsity, we control the number of the nodes inside $\mathcal{N}_{v_i}^*$ to fairly compare different methods.

³ Code for training GraphSAINT on ogbn-arxiv: https://github.com/VITA-Group/Large_Scale_GCN_Benchmarking.

⁴ Code for GNNExplainer and PGExplainer is at <https://github.com/LarsHoldijk/RE-ParameterizedExplainerForGraphNeuralNetworks>; for OrphicX is at <https://github.com/wanyugroup/cvpr2022-orphicx>; for GraphSVX is at <https://github.com/AlexDuvalinho/GraphSVX>.

D.6 Computational Infrastructure Details

All experiments in this paper are conducted on the device given in Table 7.

Table 7: Computational infrastructure details.

Device Attribute	Value
Computing infrastructure	GPU
GPU model	NVIDIA GeForce RTX 2080 Ti
GPU number	1
CUDA version	11.3

E Impact of Source and Target Embedding Dimensions

We run experiments to study the performance of LARA affected by the dimension of explanation-oriented embeddings n (the dimension of \mathbf{p}_i and \mathbf{t}_i of each node $v_i \in \mathcal{V}$) in the explainer $g(\bullet | \theta_g)$. Table 8 gives the results of Fidelity⁺ and Fidelity⁻ with $n \in \{10, 20, 30, 40\}$. Fidelity scores are averaged over the sparsity from 0.3 to 0.7 with a step size of 0.1. It is observed that the optimal setting is $n = 20$ with Fidelity⁺ of 3.72 and Fidelity⁻ of 2.32. This indicates a latent space of $n = 20$ provides an optimal solution for the hidden dimension of the explainer in LARA to learn removal-based attribution. In the case of $n \geq 20$, the redundancy of embedding causes overfit on the training dataset, which leads to a reduction of generalization fidelity. The experiments in this section are conducted on the BA-Community dataset under a unified setting of remaining factors.

Table 8: Results using different dimensions of explanation-oriented embeddings.

Dimension	10	20	30	40
Fidelity ⁺ ↑	3.44	3.72	3.42	3.30
Fidelity ⁻ ↓	2.53	2.32	2.81	2.82

F Evaluation with Ground-truth

On many synthetic datasets, ground-truth i.e., important nodes, are available. Therefore, many previous works such as [36, 24, 9] evaluate based on ground-truth. As given in the ground-truth, a node is labeled with 1 if it is important for the decision while with 0 if it is not. AUC is calculated between the given explanation scores and the ground-truth labels. We benchmark our methods with GNNExplainer, PGExplainer, and GraphSVX on synthetic datasets in Table 9. Nodes/Graphs in the test set are used for AUC evaluation. We see that LARA outperforms other methods on most of the datasets, with the exception of the X dataset where it attains the second place.

Nevertheless, ground-truth labels are not accessible in real-world datasets, such as ogbn-arxiv. Therefore, to assess the explanations in a more general way, fidelity scores are employed. Recent works on GNN explanations have begun to prioritize fidelity over ground-truth due to this reasons [19, 40]. As such, we evaluate explanation faithfulness using fidelity v.s. sparsity measures in the main paper, which is more general and challenging.

	BA-Shapes	BA-Community	Tree-Cycles	BA-2Motifs
GNNExplainer	0.448	0.441	0.612	0.487
PGExplainer	0.517	0.443	0.626	0.268
GraphSVX	0.447	0.441	0.611	0.492
LARA	0.466	0.475	0.641	0.913

Table 9: AUC of LAVA compared to other baselines on BA-Shapes, BA-Community, Tree-Cycles, and BA-2Motifs datasets. The best result is in bold.

G More Qualitative Results

We present more examples of the explanations given by LARA on node classification and graph classification tasks in Figure 8 and Figure 9, respectively.

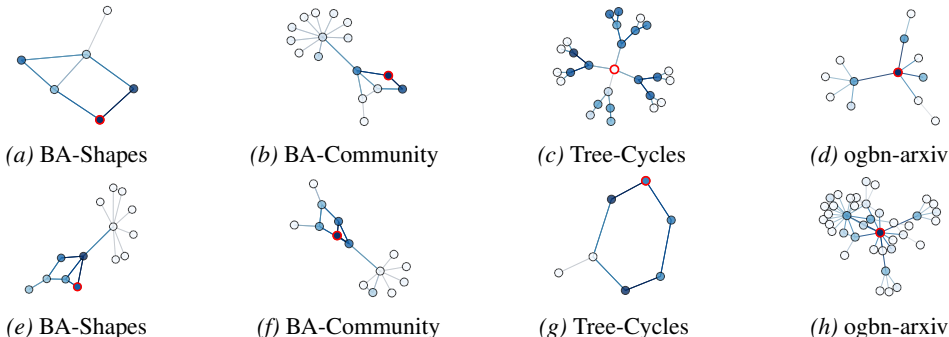


Figure 8: More qualitative results on node classification tasks. The color of the nodes indicates the importance score (explanations). Darker color refers to a higher score. Two examples are shown for each dataset. The target node (to be explained) is highlighted in red color.

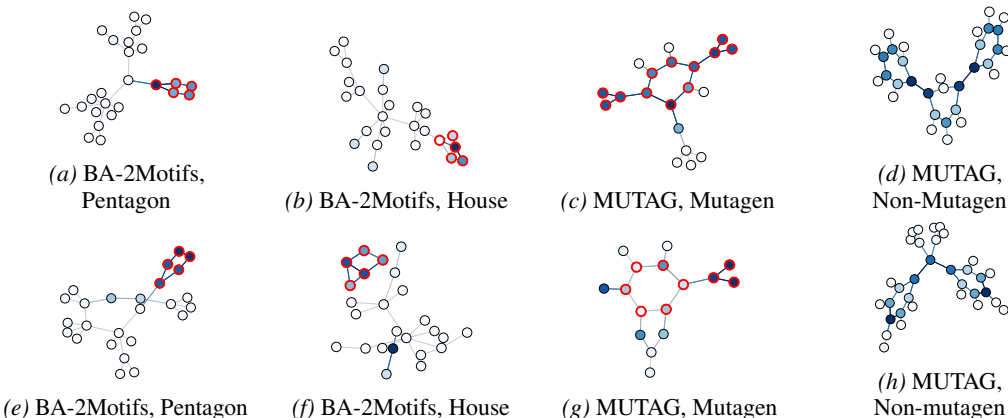


Figure 9: More qualitative results on graph classification tasks. The color of the nodes indicates the importance score (explanations). Darker color refers to a higher score. The dataset name and class of each instance are given. The ground truth motif is highlighted in red. On MUTAG, NH_2/NO_2 together with the carbon ring is the ground truth for the class mutagen. while the class Non-mutagen is without this pattern.

H Related Work

H.1 GNN Explanations

The model explanation is one of the emerging technologies in recent years due to the wide application of machine learning models, where a handful of explanation methods are proposed specifically for GNNs. Popular existing works can be divided into gradient-based, surrogate-based, decomposition-based and perturbation-based methods [38]. Gradient-based explanations follow a similar procedure as on image and text data. For instance, Pope et al. [26] propose CAM and GradCAM for graphs, which make use of the final fully-connected layer in the graph model to produce the feature map for nodes. Surrogate-based methods explain the original model via approximating it using an interpretable model [30, 15, 41]. For example, the feature weights given by the algorithm Hilbert-Schmidt Independence Criterion Lasso [34] are used as explanations for the original GNN in [15]. Decomposition-based methods back-propagate the prediction score layer by layer into the input

space following the designed decomposition rules [11, 26, 28], while perturbation-based explanations assign importance scores to nodes or edges by observing output changes when masking different input features [36, 24, 12, 37, 9, 40, 18]. Most of the perturbation-based methods [36, 24, 19, 18] learn masks of edges by minimizing the mutual information-relevant loss between the predictions with and without masking, while [37, 9, 40] provide explanatory nodes via estimating importance scores of nodes. Among these works, only a few works such as [24, 19, 18] focus on amortized explainers that can provide explanations on a test set in an inductive way after training. Different from previous amortized explainers for GNNs, we propose a novel algorithm utilizing removal-based attribution as guidance to train an explainer. In this work, we demonstrate the advantage of our method in both explanation faithfulness and efficiency compared to previous methods.

H.2 Amortized Explanations

In amortized explanation methods, a learned explainer generates explanations for a batch of instances via a forward pass [6]. [4, 17, 3, 16] showcase real-time explanations on image and tabular data. To be concrete, Jethani et al. [17] propose an algorithm FastSHAP, where an objective function is designed for an explainer to capture Shapley value distribution, achieving real-time explanations. CoRTX [4] trains an explainer using positive and negative samples by minimizing the contrastive loss. Moreover, very few labels (ground truth explanations) are used during training to boost the interpretation performance. Chen et al. [3] realize an explainer returning a distribution over selected features given the input instance. The explainer is trained by maximizing the variational approximation of mutual information between selected features and the response variable from the target model. Jethani et al. [16] propose to train a global selector and predictor jointly, where the selector (REAL-X) identifies the minimal subset of features to maximize the fidelity evaluated by a predictor model (EVAL-X). Compared to previous amortized explanations on regular data, our explainer has no constraints on input shape (unlike image or tabular data) and adapts to irregular data (graph data). Furthermore, our proposed objective function for learning removal-based attribution is designed to enable high-fidelity explanation generation. We validate its advantage from both theoretical and experimental perspectives in this work.

I Limitation and Potential Negative Social Impact

In this work, we deploy an amortized explainer to learn the removal-based attribution such that the GNN explanation can be generated fast in practical application scenarios. We remark that implementing and training the amortized explainer would have carbon emissions to the environment. Nevertheless, we wish to minimize the need for repetitive experiments with our theoretical analysis.